Supporting Information

Simple and Versatile Non-Fullerene Acceptor Based on Benzothiadiazole and Rhodanine for Organic Solar Cells

Jongho Ahn,[†,‖] Sora Oh,[†,§,‖] HyunKyung Lee,[†,‖] Sangjun Lee,[†] Chang Eun Song,*[,‡,§] Hang Ken Lee,[‡] Sang Kyu Lee,[†,§] Won-Wook So,[‡] Sang-Jin Moon,[‡,§] Eunhee Lim,[#] Won Suk Shin,*[,†,§,⊥] and Jong-Cheol Lee*[,†,§]

[†]Advanced Materials Division, Korea Research Institute of Chemical Technology (KRICT), 141 Gajeong-ro, Yuseong, Daejeon 34114, Republic of Korea

[‡]Energy Materials Research Center, Korea Research Institute of Chemical Technology (KRICT), 141 Gajeong-ro, Yuseong, Daejeon 34114, Republic of Korea

[§]Advanced Materials and Chemical Engineering, University of Science and Technology (UST), 217 Gajeongro, Yuseong, Daejeon 34113, Republic of Korea

[⊥]KU-KRICT Collaborative Research Center & Division of Display and Semiconductor Physics & Department of Advanced Materials Chemistry, Korea University, 2511 Sejong-ro, Sejong, 30019, Republic of Korea

[#]Department of Chemistry, Kyonggi University, 154-42 Gwanggyosan-ro, Yeongtong-gu, Suwon 16227, Republic of Korea

[‖]The three authors contributed equally to this paper.

*Corresponding authors. E-mail: songce@krict.re.kr (C. E. Song), shinws@krict.re.kr (W. S. Shin) and leejc@krict.re.kr (J.-C. Lee)

Experimental Sections

Instruments

The synthesized BTDT2R compound was characterized with ^{1}H NMR spectra obtained using a Bruker DPX-300 NMR Spectrometer. The UV-visible absorption was performed with a Lambda 20 (Perkin Elmer) diode array spectrophotometer. Thermogravimetric analysis (TGA) and differential scanning calorimetry (DSC) were performed under a nitrogen atmosphere at a heating rate of 10 ^{o}C/min with a Dupont 9900 analyzer. Cyclic voltammetry (CV) was performed using a Power Lab/AD instrument model system in 0.1 M solution of tetrabutylammonium hexafluorophospate (Bu_4NPF_6) in anhydrous acetonitrile as supporting electrolyte at a scan rate of 50 mVs^{-1}. A glassy carbon disk (~0.05 cm^2) coated with a thin film, an $Ag/AgNO_3$ electrode, and a platinum wire were used as working electrode, reference electrode, and counter electrode, respectively. The atomic force microscope (AFM) (Multimode IIIa, Digital Instruments) was operated in tapping mode to acquire images of the surfaces of photoactive films. Conventional transmission electron microscopy (TEM) of the optimized photoactive layers was performed using a JEOL JEM-2200FS operated at 200 kV.

Materials

P3HT and PTB7-Th were purchased from Rieke Metals and 1-material, respectively. The solvents were purchased from Sigma-Aldrich and used without special treatment. PPDT2FBT was synthesized following previously reported method.[S1]

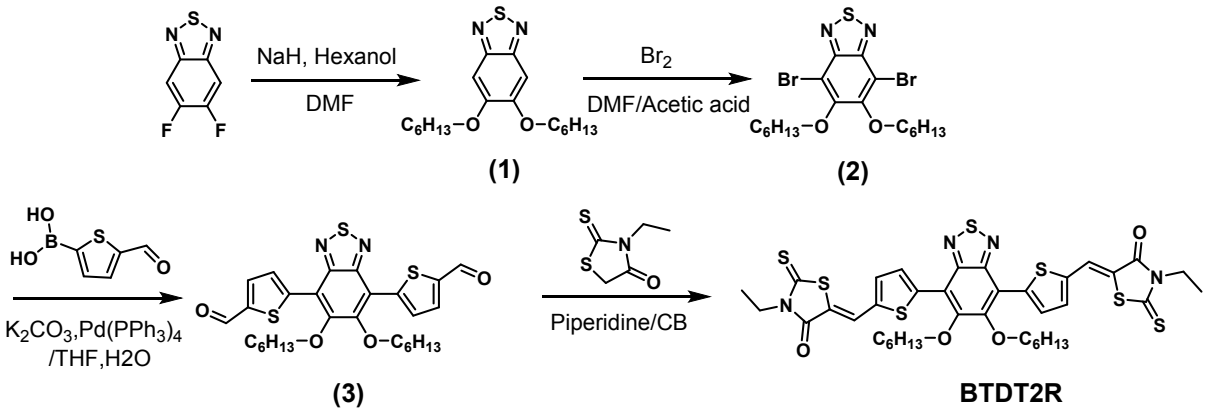

Scheme S1. Synthetic scheme of BTDT2R.

5,6-bis(hexyloxy)benzo[c][1,2,5]thiadiazole **(1)**

1-hexanol (255mg, 14.5 mmol) was added into 2-neck round bottom flask contained 50ml of anhydrous tetrahydrofuran under argon atmosphere. After cooling down to 0 ^{o}C, sodium hydride (60% dispersion in paraffin) (0.7 g, 17.4 mmol) was added as one portion. After being stirred for 1h at 0 ^{o}C, 5,6-difluorobenzo[c][1,2,5]thiadiazole (1.0 g, 5.8 mmol) was added and reaction mixture was refluxed overnight. Then mixture was bought to 0 ^{o}C and slowly quenched by dropwise addition of 50 ml water and product was extracted with ethyl acetate. The organic extraction was dried over anhydrous magnesium sulfate and then concentrated. The crude product was purified by silica gel column with dichloromethane (30%) in hexane as eluent, yielding 1 (1.8 g, 78%) as a white solid.

^{1}H NMR (400 MHz, $CDCl_3$): δ (ppm) 7.13 (s, 2H), 4.09 (t, J = 6.5 Hz, 4H), 1.94-1.87 (m, 4H), 1.56-1.26 (m, 12H), 0.89-0.85 (m, 6H). ^{13}C NMR (500 MHz, $CDCl_3$): δ (ppm) 154.1; 151.40; 98.4; 69.1; 31.9; 29.72; 26.0; 22.7; 14.1.

MS (EI): Calculated m/z 336.19; found M+ 336.40.

4,7-dibromo-5,6-bis(hexyloxy)benzo[c][1,2,5]thiadiazole (2)

To the stirred solution of 5,6-bis(hexyloxy)benzo[c][1,2,5]thiadiazole (1) (1.8g, 4.9 mmol) in dichloromethane: (40mL) acetic acid (10ml) and bromine (2.4g,14.8 mmol) was added at room temperature and reaction mass was refluxed overnight. Reaction mass was bought to 0 ^{o}C and slowly quenched with sodium thiosulphate solution and extracted with chloroform (10ml x 3). The organic extraction was dried over anhydrous magnesium sulfate and then concentrated. The crude product was purified by silica gel column with dichloromethane (30%) in hexane as eluent, yielding 2 (2.8 g, 84%) as off white solid.

^{1}H NMR (400 MHz, $CDCl_3$): δ (ppm) 4.16 (t, *J* = 6.64 Hz, 4H); 1.90-1.86 (m, 4H); 1.56-1.50 (m, 12H), 0.88 (t, *J* = 6.6 Hz, 6H). ^{13}C NMR (500 MHz, $CDCl_3$): δ (ppm) 154.54; 150.4; 106.26; 75.17; 31.93; 29.70; 26.0, 22.7; 14.11.

MS (EI): Calculated m/z : 494.01; found M+ 494.29

5,5'-(5,6-bis(hexyloxy)benzo[c][1,2,5]thiadiazole-4,7-diyl)bis(thiophene-2-carbaldehyde) (3)

A mixture of 2 (0.8 g, 1.5 mmol), (5-formylthiophene-2-yl)boronic acid (2.3 g, 14.7 mmol), $Pd(PPh_3)_4$ (173 mg, 0.15 mmol), K2CO3 (1.1g, 7.5 mmol) was weighed into a two-neck round bottom flask and degassed for 15 minutes. Degassed THF (15 mL) and water (4.5 mL) were added, then the reaction mixture was purged with argon and allowed to stir at 65 ^{o}C for 24 hours. The solvent was evaporated under vacuum and the residue on activated neutral alumina column chromatography (3% ethyl acetate in hexane) yielded the product as a white amorphous solid (860 mg, 95%).

1H NMR (400 MHz, $CDCl_3$): δ (ppm) 9.89 (s, 2H), 7.94 (d, J = 7.2 Hz 1H), 7.84 (d, J = 7.1 Hz, 2H), 4.06 (t, *J* = 6.64 Hz, 4H) 1.90-1.86 (m, 4H); 1.56-1.50 (m, 12H), 0.88 (t, *J* = 6.6 Hz, 6H). ^{13}C NMR (500 MHz, $CDCl_3$): δ (ppm) 182.47, 148.92, 146.42, 144.21, 141.82, 138.95, 129.44, 115.96, 75.17; 31.93; 29.70; 26.0, 22.7; 14.11.

MS (EI): Calculated m/z : 556.15; found M+ 556.75

BTDT2R

A mixture of substance 3 (143 mg, 0.3 mmol), ethyl rhodamine (124 mg. 0.8 mmol), piperidine (5 drops) and chlorobenzene (10 ml) was stirred at 60 °C for 8 h. The reaction mixture was then cooled to r.t. and filtered. The residue was purified using column chromatography on silica gel employing methylene chloride/hexane (3:1) as an eluent, yielding a red-colored solid (262 mg, 86%).

^1H NMR (400 MHz, $CDCl_3$) δ (ppm): 8.83 (d, J=4.3, 2H), 7.93 (s, 2H), 7.54 (d, J=4.4, 2H), 4.23 (m, 8H), 2.10 (m, 4H), 1.50-1.45 (m, 12H), 1.38 (t, *J* = 6.30 Hz, 4H), 0.93 (t, *J* = 6.8 Hz, 6H). ^{13}C NMR (500 MHz, $CDCl_3$): δ (ppm) 189.2, 166.12, 146.45, 144.03, 142.97, 137.52, 130.14, 128.77, 122.04, 155.96, 75.13, 40.07, 31.99, 29.63, 26.41, 22.74, 14.10, 11.63.

MS (EI): Calculated m/z : 842.13; found M+ 843.20.

Hole and electron mobility measurements

The hole and electron mobility of active films were measured by using SCLC method. The hole-only (ITO/PEDOT:PSS/active film/Au) and electron-only (ITO/ZnO NPs/PEIE/active

film/Ca/Al) devices were fabricated. The charge carrier mobility were determined by fitting dark *J-V* measurements in the 0-8 V range into space charge limited form and mobility (μ) calculated using equation $J = 9\varepsilon_0\varepsilon_r\mu V^2/8L^3$, where J = current density, ε_r = dielectric constant of the transport medium, ε_0 = permittivity of free space (8.85×10^{-12} F m^{-1}), V = internal voltage and L = active film thickness, respectively.

GIWAXS Characterization.

2D-GIWAX measurements were performed on the PLS–II 3C beam line at the Pohang Accelerator Laboratory in Republic of Korea. The active materials were coated on silicon/ZnO NPs/PEIE substrate with optimized device fabrication conditions. The monochromatic X-ray beam with intensity 11 keV was adjusted with incident angle 0.11^o -0.14^o on sample with irradiation time 5-20 sec, selected to maximize the scattering intensity from the active films. The scattered X-ray patterns were recorded with charge coupled device (CCD) detector.

Near-Edge X-Ray Absorption of Fine Structure (NEXAFS)[S2]

NEXAFS measurements were performed at 4D PES beamline of PAL in Repulic of Korea. We used the total electron yield (TEY) detection mode for the NEXAFS spectra by recording the sample current normalized to a signal current, which was measured simultaneously using a gold mesh in ultrahigh vacuum ($<10^{-9}$ Torr). In this case, a *p*-polarized (≈85%) synchrotron photon beam had an energy in the range of 270–325 eV and a spectral energy resolution of ΔE = 150 meV. In particular, NEXAFS can measure the average orientation of the π-conjugated planes in organic semiconductors by collecting carbon K-edge spectra obtained from various

angles of incidence of the synchrotron photon beam from the surface plane. Furthermore, detailed structural information, such as the tilting angle of the conjugated planes, can be derived from the spectra. The features in the NEXAFS spectra are assigned to the π* (C=C) orbital at 285.4 eV. To determine the tilt angle (α) between the C=C double bond in the conjugated planes and the Si/ZnO NPs/PEIE substrate surface, a fourfold symmetry of the substrate was used with the photon beam, which had a beam size of 0.1 × 0.3 mm^2. The peak intensities of the π* (C=C) orbital in the NEXAFS spectra were then fitted by the following Equation S1

$$I_v \propto \left[\frac{P}{3}\left\{1+\frac{1}{2}(3cos^2\theta-1)(3cos^2\alpha-1)\right\}+\frac{(1-P)}{2}sin^2\alpha\right] \quad \text{(S1)}$$

where θ is the polarization angle of the incident synchrotron light with respect to the normal to the surface, and P = 0.85 is used for the degree of polarization. In addition, the dichroic ratio (R), which represents an average chain conformation of films, was calculated using Equation S2

$$R = \frac{/(90°)-/(0°)}{/(90°)+/(0°)} \quad \text{(S2)}$$

which is the difference between the intensities at θ = 90° and 0°, divided by their sum. The value of R varies from +0.7 (for horizontal π* orbital and α = 90°), to 0 (for random orientation, known as magic angle α = 54.7°) and −1 (for a vertical π* orbital and α = 0°): a more positive R signifies a larger average tilting angle of the transition dipole away from the substrate.

Reference

(S1) T. L. Nguyen, H. Choi, S.-J. Ko, M. A. Uddin, B. Walker, S. Yum, J.-E. Jeong, M. H. Yun, T. J. Shin, S. Hwang, J. Y. Kim, H. Y. Woo, *Energy Environ. Sci*. **2014**, *7*, 3040-3051.

(S2) H. I. Kim, M. Kim, C. W. Park, H. U. Kim, H.-K. Lee, T. Park, *Chem. Mater*. **2017**, *29*, 6793-6798.

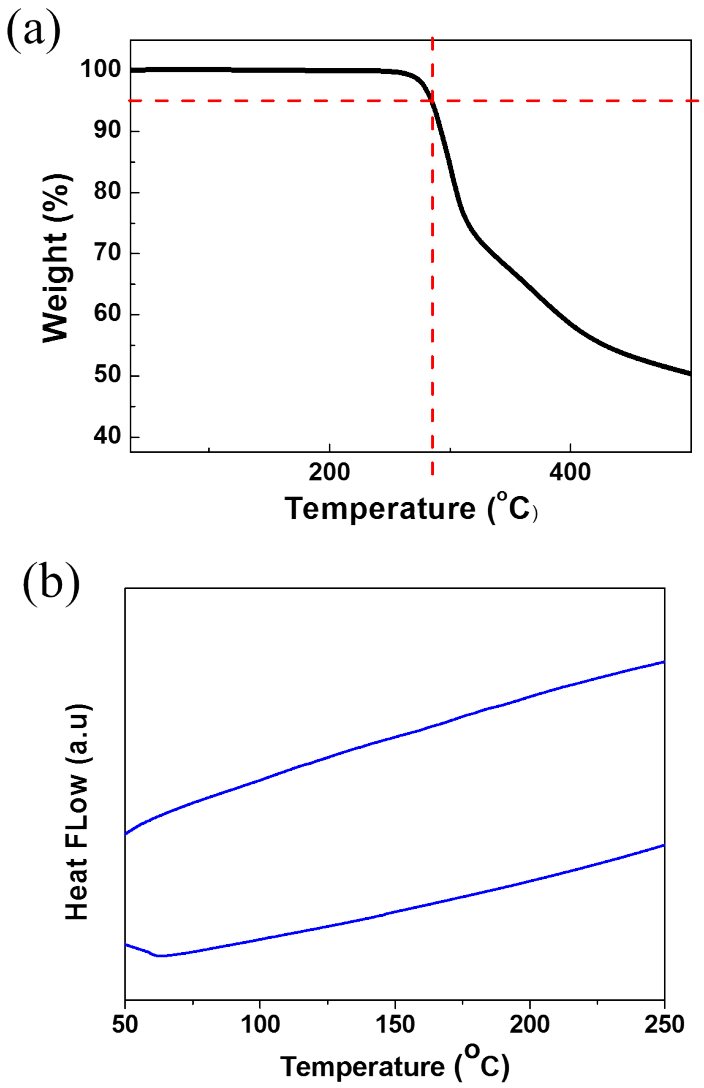

Figure S1. (a) TGA (b) DSC curve of BTDT2R.

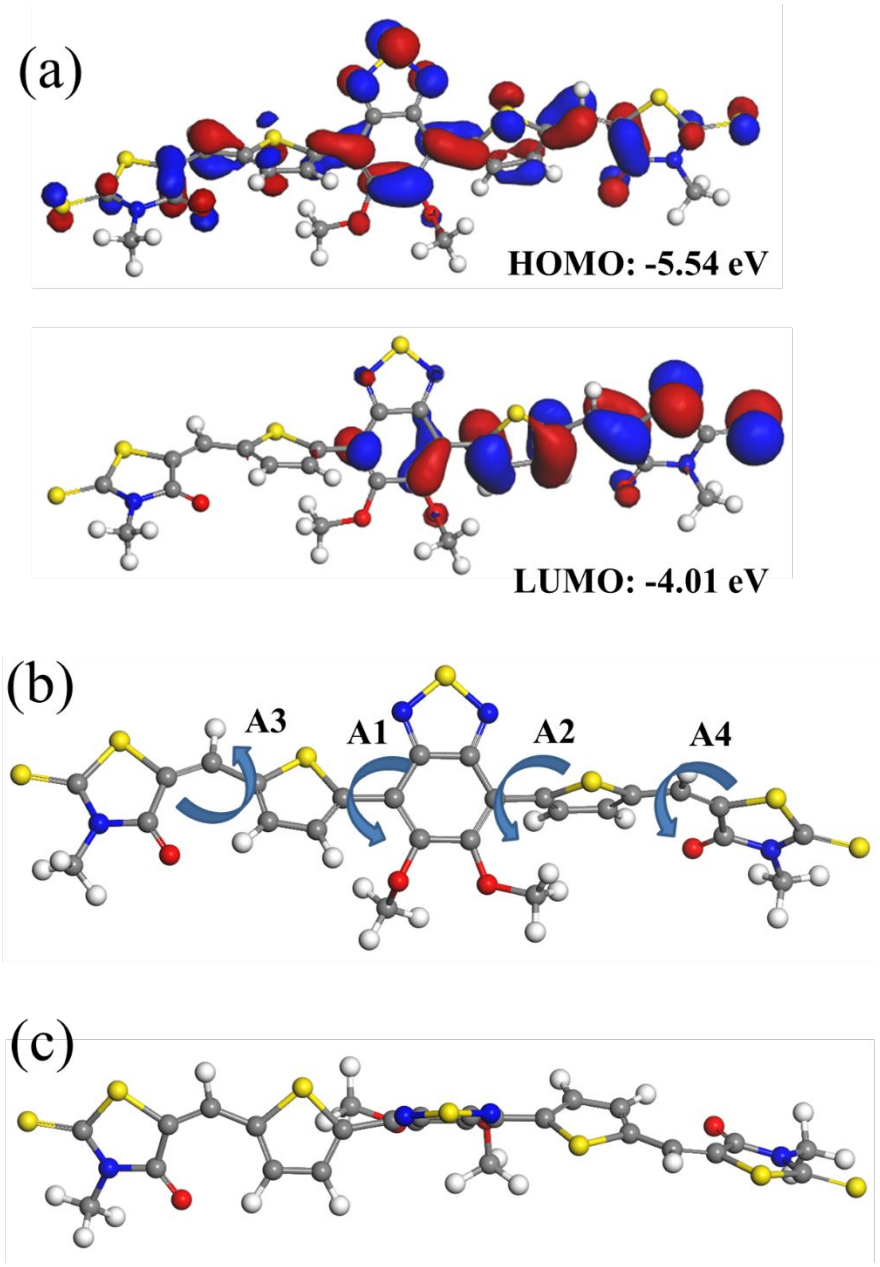

Figure S2. (a) Molecular energy levels, (b) top view, and (c) side view of the optimized geometry of BTDT2R calculated by DFT at the B3LYP/6-31G(d, p) level.

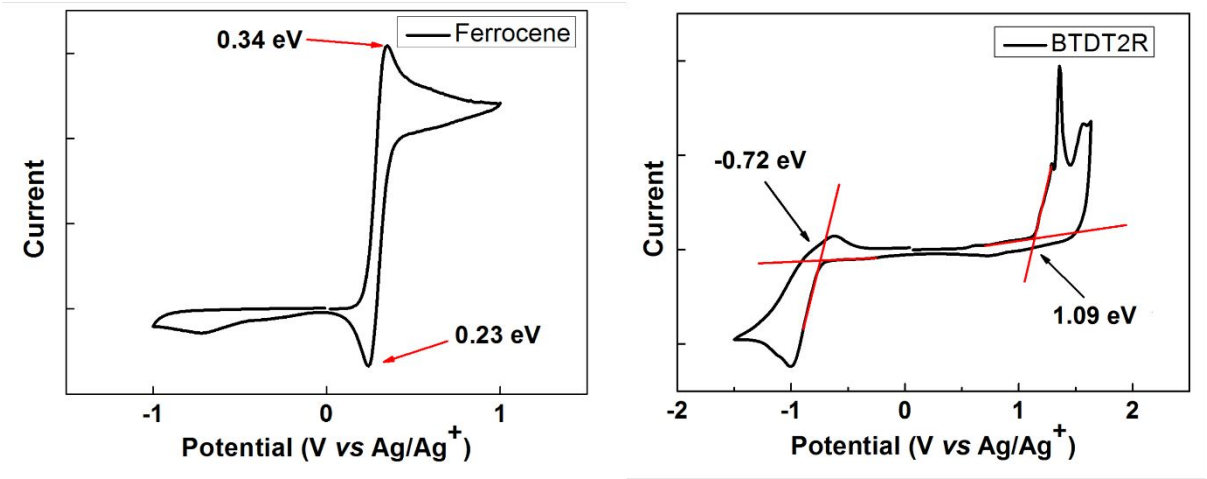

Figure S3. Cyclic voltammograms of BTDT2R.

Table S1. Photovoltaic properties of P3HT(P1):BTDT2R with different thermal annealing temperatures and solvent vapor annealing systems under AM 1.5G illumination.[a)]

Polymer Donor	**Annealing**	V_{OC} **[V]**	J_{SC} **[mA/cm^2]**	***FF*** **[%]**	**PCE [%]**
P3HT	W/O	0.88	6.44	48	2.74
	90^{o}C, 10min	0.78	9.31	58	4.19
	120^{o}C, 10min	0.76	9.75	59	4.34
	150^{o}C, 10min	0.75	9.37	59	4.15
	CF, 15s	0.80	9.13	62	4.58
	THF, 15s	0.81	9.55	64	4.95
	DCM, 15s	0.81	9.42	67	5.09

[a)]The devices architecture is ITO/ZnO NPs/PEIE/ P3HT:BTDT2R(d = ~100nm)/MoO_X/Ag.

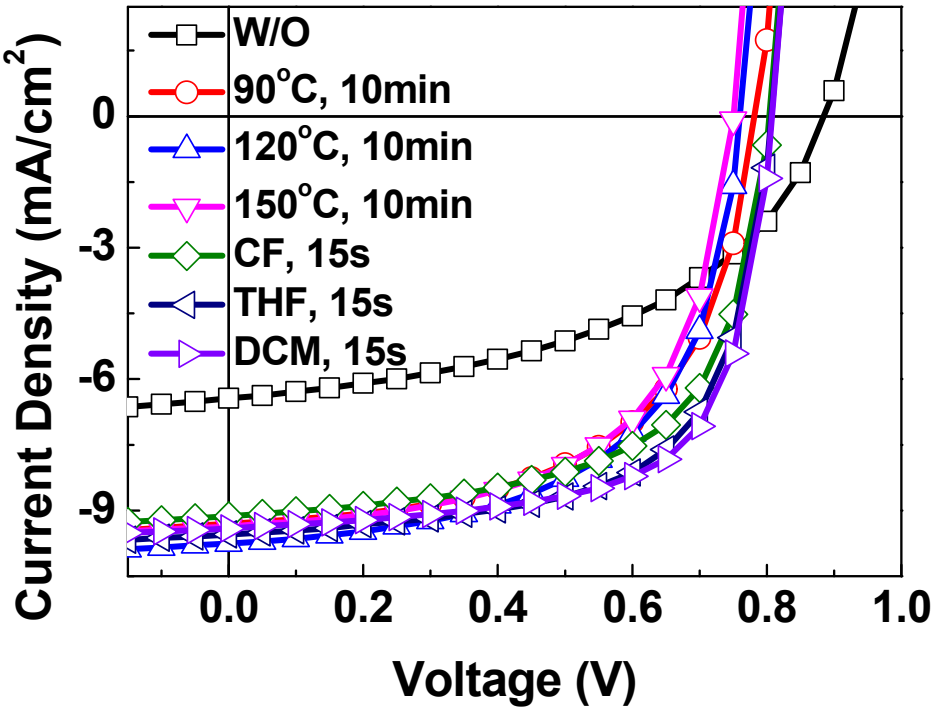

Figure S4. *J-V* curves of P3HT(P1):BTDT2R-based OSCs without and with different thermal annealing temperature and solvent vapor annealing by different solvents.

Table S2. Photovoltaic properties of PPDT2FBT(P2):BTDT2R with different thermal annealing temperatures and solvent vapor annealing systems under AM 1.5G illumination.[a)]

Polymer Donor	Annealing	V_{OC} [V]	J_{SC} [mA/cm^2]	*FF* [%]	PCE [%]
PPDT2FBT	W/O	1.07	8.37	38	3.39
	90^{o}C, 10min	1.05	10.52	44	4.89
	120^{o}C, 10min	1.02	11.47	50	5.84
	150^{o}C, 10min	0.98	10.99	53	5.74
	CF, 15s	1.07	10.58	57	6.52
	THF, 15s	1.07	10.98	57	6.74
	DCM, 15s	1.07	11.23	57	6.90

[a)]The devices architecture is ITO/ZnO NPs/PEIE/ PPDT2FBT:BTDT2R(*d* = ~100nm)/MoO_X/Ag.

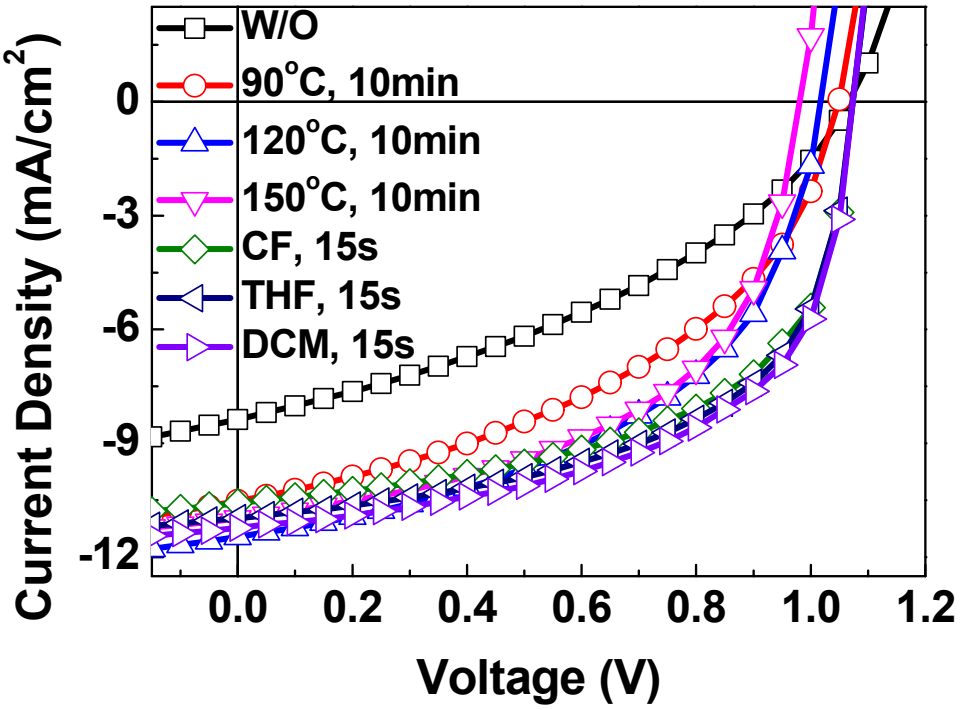

Figure S5. *J-V* curves of PPDT2FBT(P2):BTDT2R-based OSCs without and with different thermal annealing temperature and solvent vapor annealing by different solvents.

Table S3. Photovoltaic properties of PTB7-Th(P3):BTDT2R with different thermal annealing temperatures and solvent vapor annealing systems under AM 1.5G illumination.[a)]

Polymer Donor	**Annealing**	V_{OC} **[V]**	J_{SC} **[mA/cm^2]**	***FF*** **[%]**	**PCE [%]**
PTB7-Th	W/O	1.06	12.06	40	5.03
	90^{o}C, 10min	1.03	12.97	42	5.63
	120^{o}C, 10min	1.05	12.60	44	5.85
	150^{o}C, 10min	1.04	11.13	46	5.33
	CF, 15s	1.04	8.50	46	4.01
	THF, 15s	1.05	13.41	53	7.51
	DCM, 15s	1.06	13.52	57	8.19

[a)]The devices architecture is ITO/ZnO NPs/PEIE/ PTB7-Th:BTDT2R(d = ~100nm)/MoO_X/Ag.

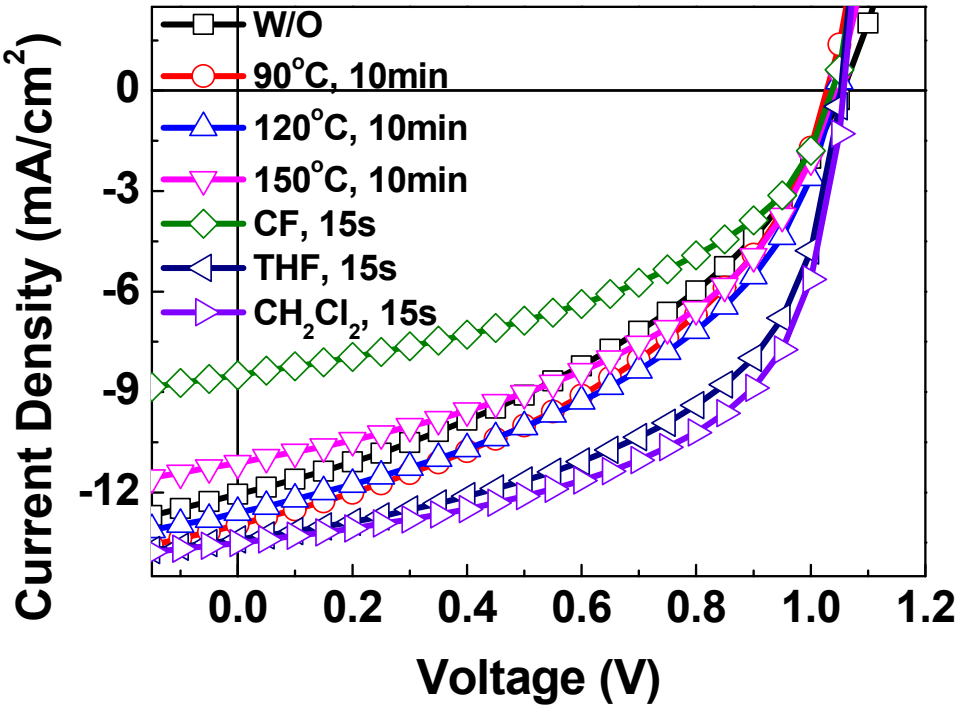

Figure S6. *J-V* curves of PTB7-Th(P3):BTDT2R-based OSCs without and with different thermal annealing temperature and solvent vapor annealing by different solvents.

Table S4. Photovoltaic properties of P1:BTDT2R with different blend ratio under AM 1.5G illumination.[a)]

Polymer Donor	Weight Ratio	Annealing	V_{OC} [V]	J_{SC} [mA/cm^2]	*FF* [%]	PCE [%]
P3HT (P1)	1:1	W/O	0.89	4.65 (4.60)[c)]	36	1.48
		SVA[b)]	0.81	8.18 (8.03)[c)]	61	4.01
	1:2	W/O	0.88	6.44 (6.27)[c)]	48	2.74
		SVA[b)]	0.81	9.42 (9.28)[c)]	67	5.09
	1:3	W/O	0.89	6.52 (6.37)[c)]	51	2.96
		SVA[b)]	0.81	9.22 (9.11)[c)]	62	4.60

[a)]The devices architecture is ITO/ZnO NPs/PEIE/ P3HT:BTDT2R(d = ~100nm)/MoO_X/Ag.

[b)]The photoactive layer is annealed by solvent vapor annealing (SVA) using DCM, for 15s.

[c)]Calculated J_{SC} values from EQE curves.

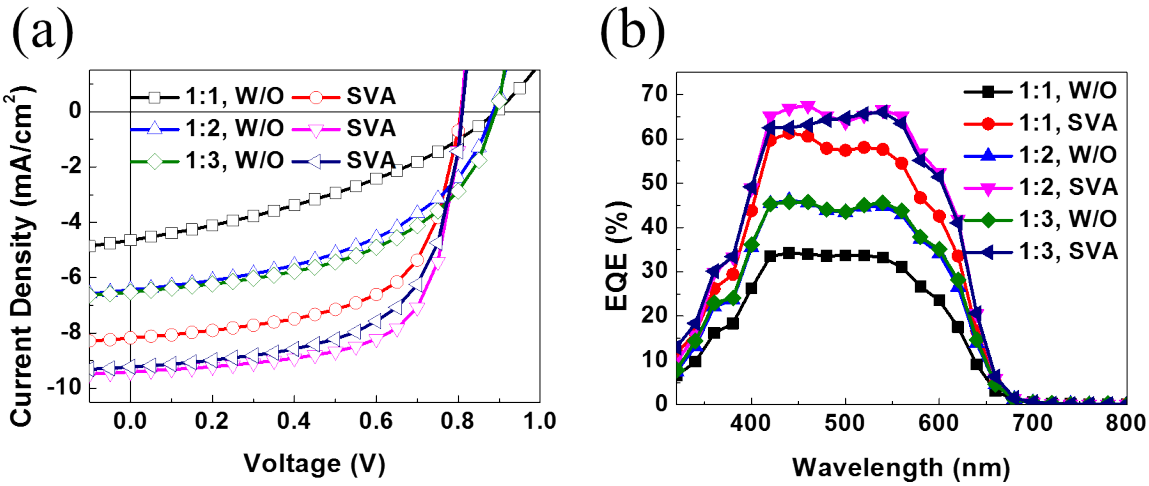

Figure S7. (a) *J-V* curves and (b) EQE curves of P1:BTDT2R-based OSCs with different blend ratios.

Table S5. Photovoltaic properties of P2:BTDT2R with different blend ratio under AM 1.5G illumination.[a)]

Polymer Donor	Weight Ratio	Annealing	V_{OC} [V]	J_{SC} [mA/cm^2]	*FF* [%]	PCE [%]
PPDT2FBT (P2)	1:1	W/O	1.09	6.64 (6.51)[c)]	34	2.47
		SVA[b)]	1.06	7.46 (7.32)[c)]	46	3.64
	1:2	W/O	1.07	8.37 (8.24)[c)]	38	3.39
		SVA[b)]	1.07	11.23 (11.04)[c)]	57	6.90
	1:3	W/O	1.06	8.30 (8.21)[c)]	41	3.60
		SVA[b)]	1.06	10.29 (10.11)[c)]	54	5.87

[a)]The devices architecture is ITO/ZnO NPs/PEIE/ PPDT2FBT:BTDT2R(*d* = ~100nm)/MoO_X/Ag.

[b)]The photoactive layer is annealed by solvent vapor annealing (SVA) using DCM, for 15s.

[c)]Calculated J_{SC} values from EQE curves.

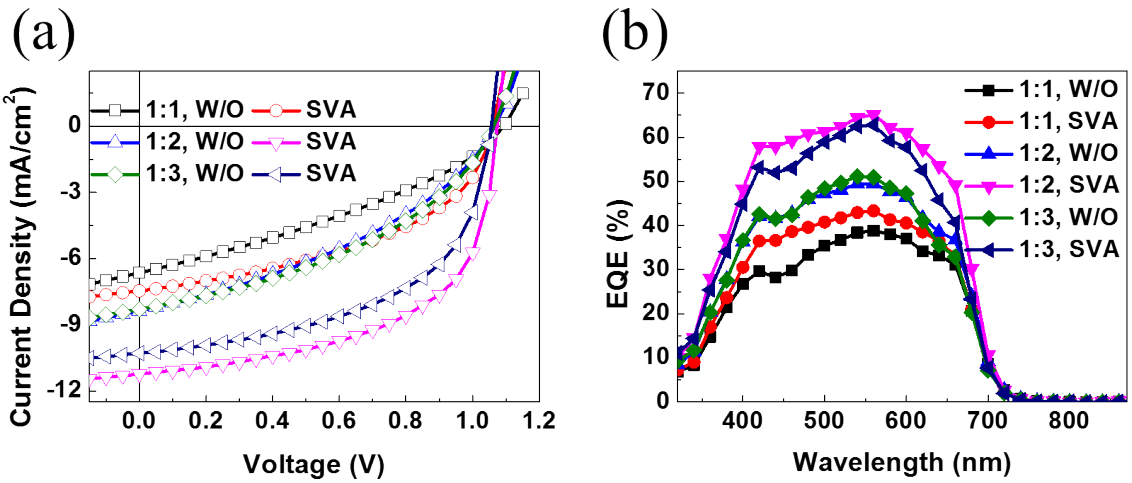

Figure S8. (a) *J-V* curves and (b) EQE curves of P2:BTDT2R-based OSCs with different blend ratios.

Table S6. Photovoltaic properties of P3:BTDT2R with different blend ratio under AM 1.5G illumination.[a)]

Polymer Donor	Weight Ratio	Annealing	V_{OC} [V]	J_{SC} [mA/cm^2]	*FF* [%]	PCE [%]
PTB7-Th (P3)	1:1	W/O	1.05	10.29 (10.08)[c)]	34	3.70
		SVA[b)]	1.04	11.57 (11.39)[c)]	36	4.38
	1:2	W/O	1.06	12.06 (11.90)[c)]	40	5.03
		SVA[b)]	1.06	13.52 (13.14)[c)]	57	8.19
	1:3	W/O	1.06	11.60 (11.42)[c)]	35	4.35
		SVA[b)]	1.05	13.14 (13.04)[c)]	57	7.94

[a)]The devices architecture is ITO/ZnO NPs/PEIE/ PTB7-Th:BTDT2R(d = ~100nm)/MoO_X/Ag.

[b)]The photoactive layer is annealed by solvent vapor annealing (SVA) using DCM, for 15s.

[c)]Calculated J_{SC} values from EQE curves.

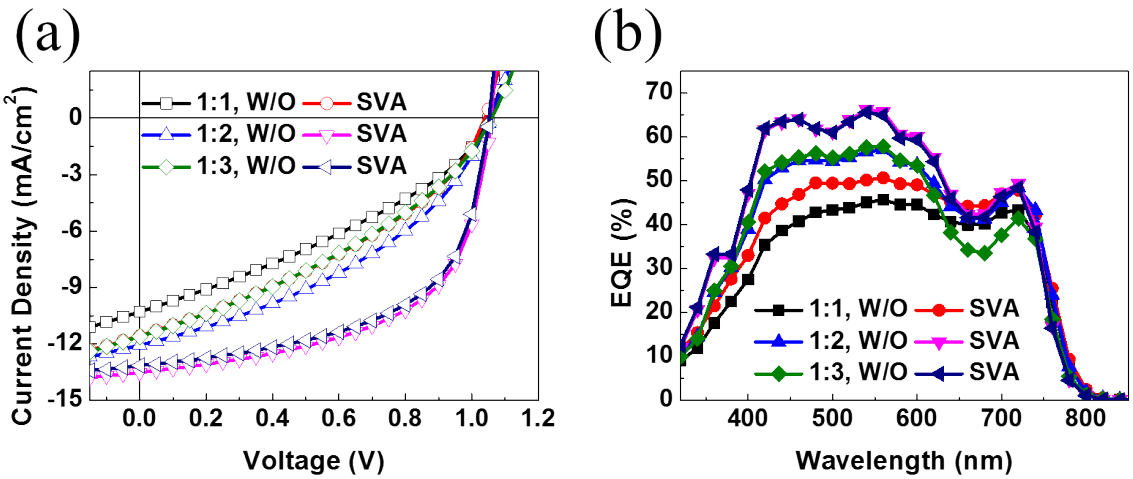

Figure S9. (a) *J-V* curves and (b) EQE curves of P3:BTDT2R-based OSCs with different blend ratios.

Table S7. Photovoltaic properties of P1:BTDT2R with various CH_2Cl_2 vapor annealing time under AM 1.5G illumination.[a)]

Polymer Donor	SVA Time[b)]	V_{OC} [V]	J_{SC} [mA/cm^2]	*FF* [%]	PCE [%]
P3HT	0 s	0.88	6.44 (6.27)[c)]	48	2.74
	7 s	0.84	7.90 (7.80)[c)]	60	3.97
	15 s	0.81	9.42 (9.28)[c)]	67	5.09
	25 s	0.81	9.15 (9.03)[c)]	65	4.78
	40 s	0.80	8.78 (8.69)[c)]	65	4.60
	60 s	0.80	8.66 (8.49)[c)]	65	4.51
	90 s	0.80	8.32 (8.17)[c)]	64	4.28

[a)]The devices architecture is ITO/ZnO NPs/PEIE/Polymer Donor:BTDT2R(*d* = ~100nm)/MoO_X/Ag.

[b)]All devices are annealed by DCM.

[c)]The value is calculated from EQE graph.

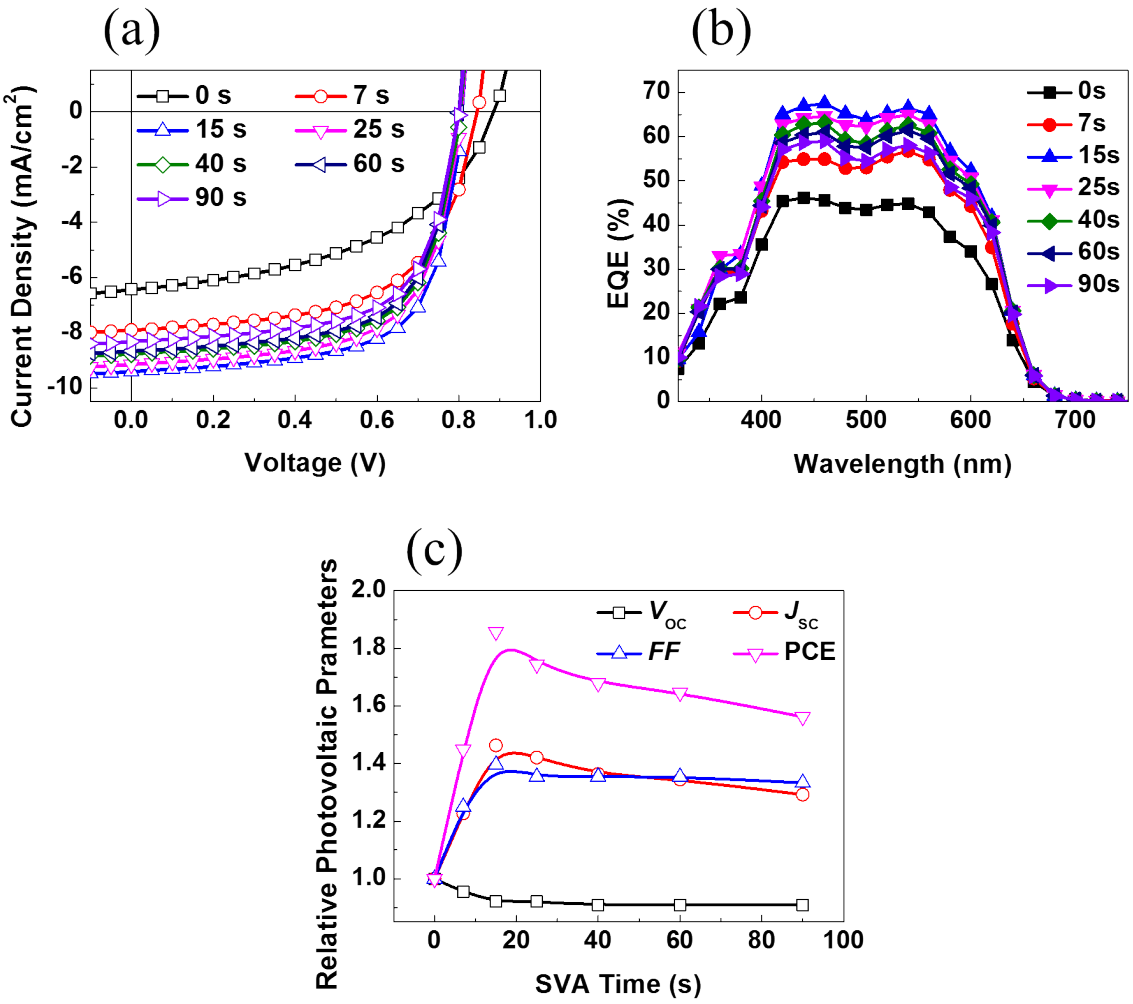

Figure S10. (a) *J-V* and (b) EQE curves of P3HT(P1):BTDT2R-based OSCs with solvent vapor annealing times by using the DCM solvent. (c) Photovoltaic parameters (V_{OC}, J_{SC}, *FF* and PCE) *vs* SVA time.

Table S8. Photovoltaic properties of P2:BTDT2R with various CH_2Cl_2 vapor annealing time under AM 1.5G illumination.[a)]

Polymer Donor	SVA Time[b)]	V_{OC} [V]	J_{SC} [mA/cm^2]	*FF* [%]	PCE [%]
PPDT2FBT	0 s	1.07	8.37 (8.24)[c)]	38	3.39
	7 s	1.06	10.47 (10.28)[c)]	46	5.13
	15 s	1.07	11.23 (11.04)[c)]	57	6.90
	25 s	1.06	10.52 (10.34)[c)]	55	6.13
	40 s	1.05	10.19 (10.02)[c)]	53	5.75
	60 s	1.05	9.39 (9.30)[c)]	55	5.40
	90 s	1.03	7.81 (7.78)[c)]	55	4.40

[a)]The devices architecture is ITO/ZnO NPs/PEIE/Polymer Donor:BTDT2R(*d* = ~100nm)/MoO_X/Ag.

[b)]All devices are annealed by DCM.

[c)]The value is calculated from EQE graph.

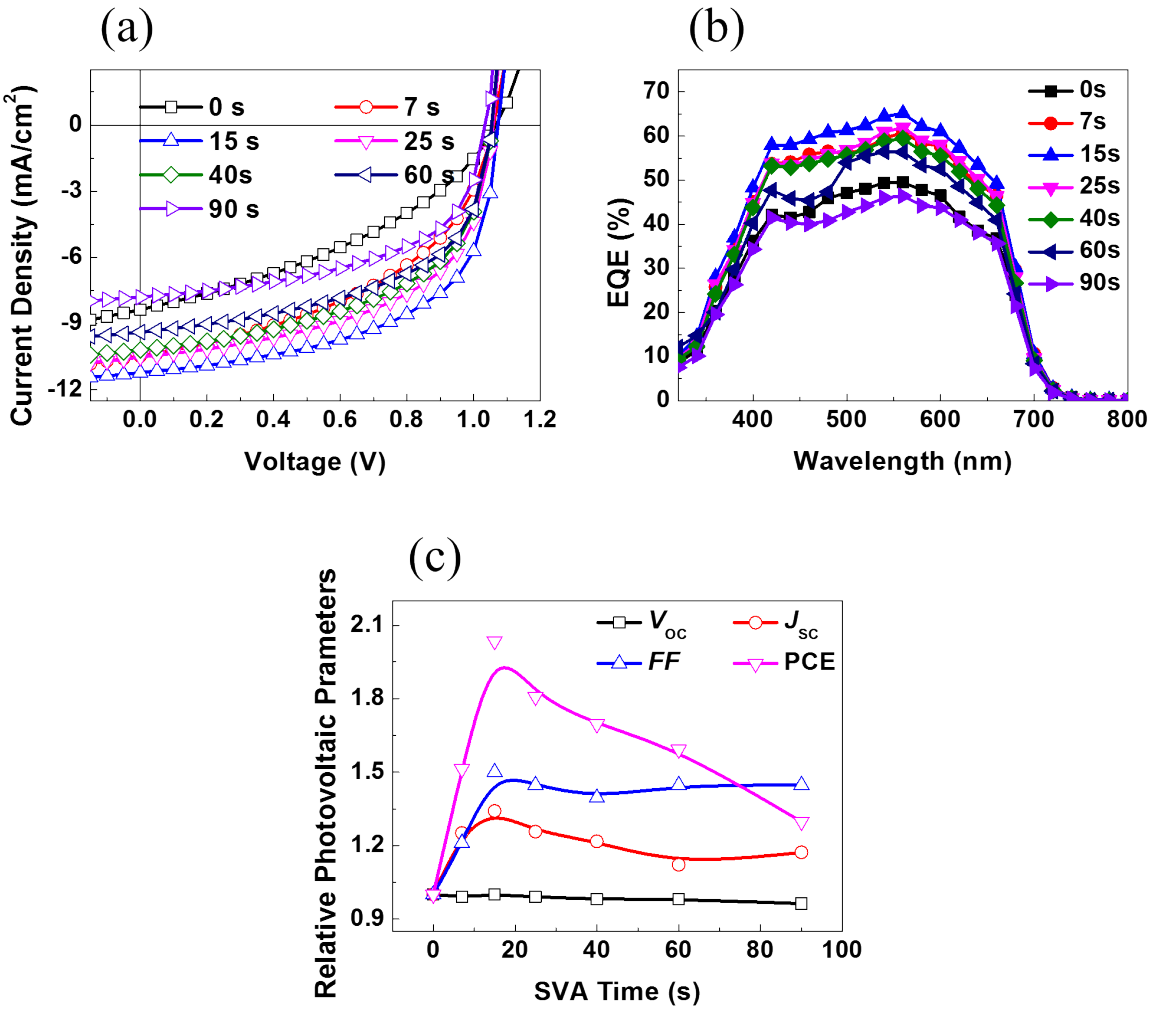

Figure S11. (a) *J-V* and (b) EQE curves of PPDT2FBT(P2):BTDT2R-based OSCs with solvent vapor annealing times by using the DCM solvent. (c) Photovoltaic parameters (V_{OC}, J_{SC}, *FF* and PCE) *vs* SVA time.

Table S9. Photovoltaic properties of P3:BTDT2R with various CH_2Cl_2 vapor annealing time under AM 1.5G illumination.[a)]

Polymer Donor	SVA Time[b)]	V_{OC} [V]	J_{SC} [mA/cm^2]	*FF* [%]	PCE [%]
PTB7-Th	0 s	1.06	12.06 (11.90)[c)]	40	5.03
	7 s	1.05	12.79 (12.60)[c)]	42	5.66
	15 s	1.06	13.52 (13.14)[c)]	57	8.19
	25 s	1.03	13.24 (13.01)[c)]	59	8.05
	40 s	1.04	12.41 (12.27)[c)]	60	7.79
	60 s	1.03	12.15 (12.04)[c)]	61	7.54
	90 s	1.04	11.95 (11.77)[c)]	59	7.34

[a)]The devices architecture is ITO/ZnO NPs/PEIE/Polymer Donor:BTDT2R(*d* = ~100nm)/MoO_X/Ag.

[b)]All devices are annealed by DCM.

[c)]The value is calculated from EQE graph.

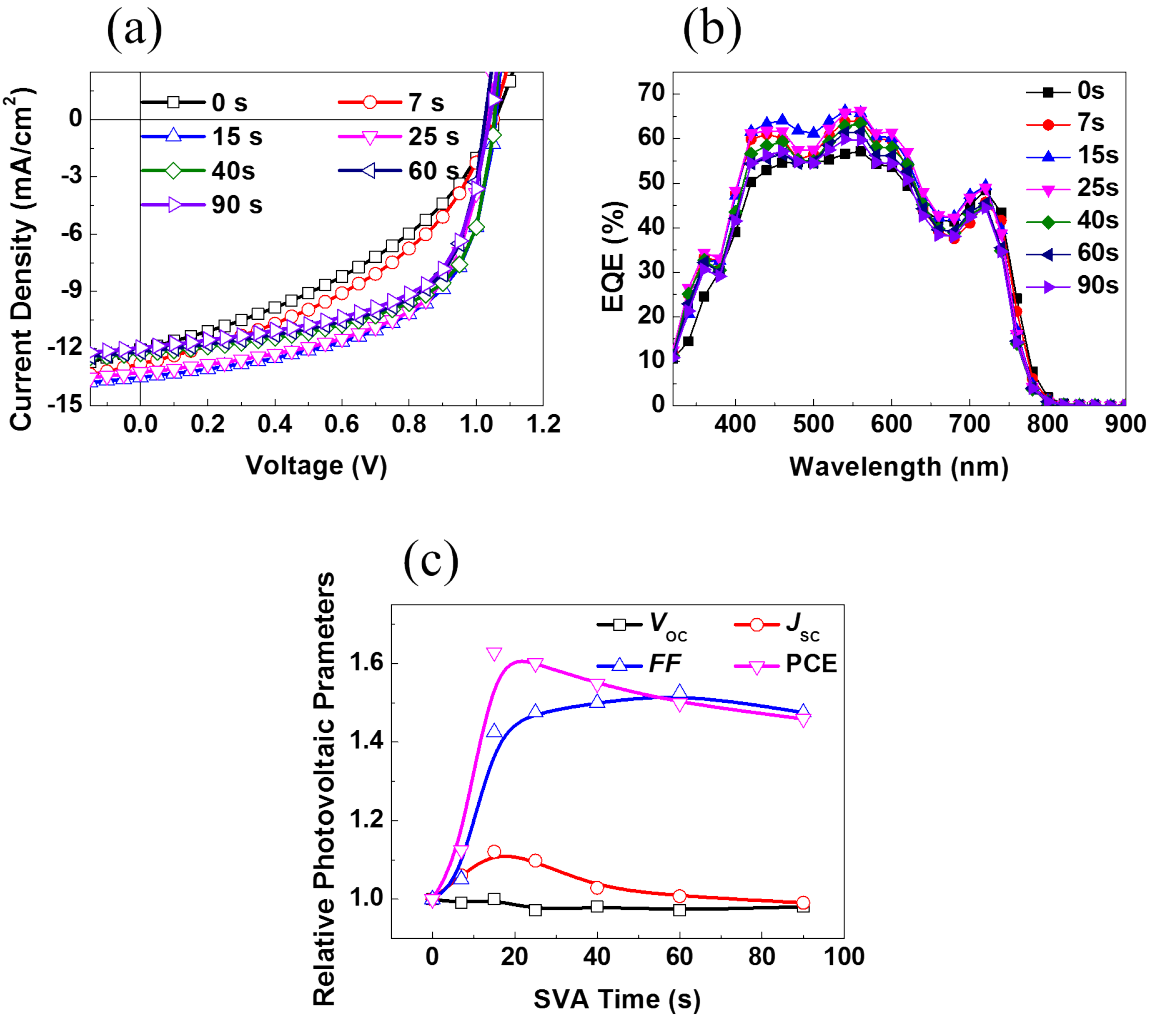

Figure S12. (a) *J*-*V* and (b) EQE curves of PTB7-Th(P3):BTDT2R-based OSCs with solvent vapor annealing times by using the DCM solvent. (c) Photovoltaic parameters (V_{OC}, J_{SC}, *FF* and PCE) *vs* SVA time.

Table S10. Photovoltaic properties of polymer:BTDT2R with different photoactive layer thickness under AM 1.5G illumination.[a)]

Polymer Donor	*d* [nm]	V_{OC} [V]	J_{SC} [mA/cm^2]	*FF* [%]	PCE [%]
P3HT	~230	0.81	8.18	61	4.01
	~160	0.81	8.53	64	4.43
	~100	0.81	9.42	67	5.09
	~70	0.81	8.63	67	4.66
PPDT2FBT	~230	1.05	10.36	52	5.73
	~160	1.07	10.74	54	6.20
	~100	1.07	11.23	57	6.90
	~70	1.07	10.57	58	6.49
PTB7-Th	~230	1.04	11.85	51	6.23
	~160	1.05	13.02	53	7.26
	~100	1.06	13.52	57	8.19
	~70	1.05	11.76	61	7.52

[a)]The devices architecture is ITO/ZnO NPs/PEIE/Polymer Donor:BTDT2R/MoO_X/Ag and all devices are annealed by DCM for 15s.

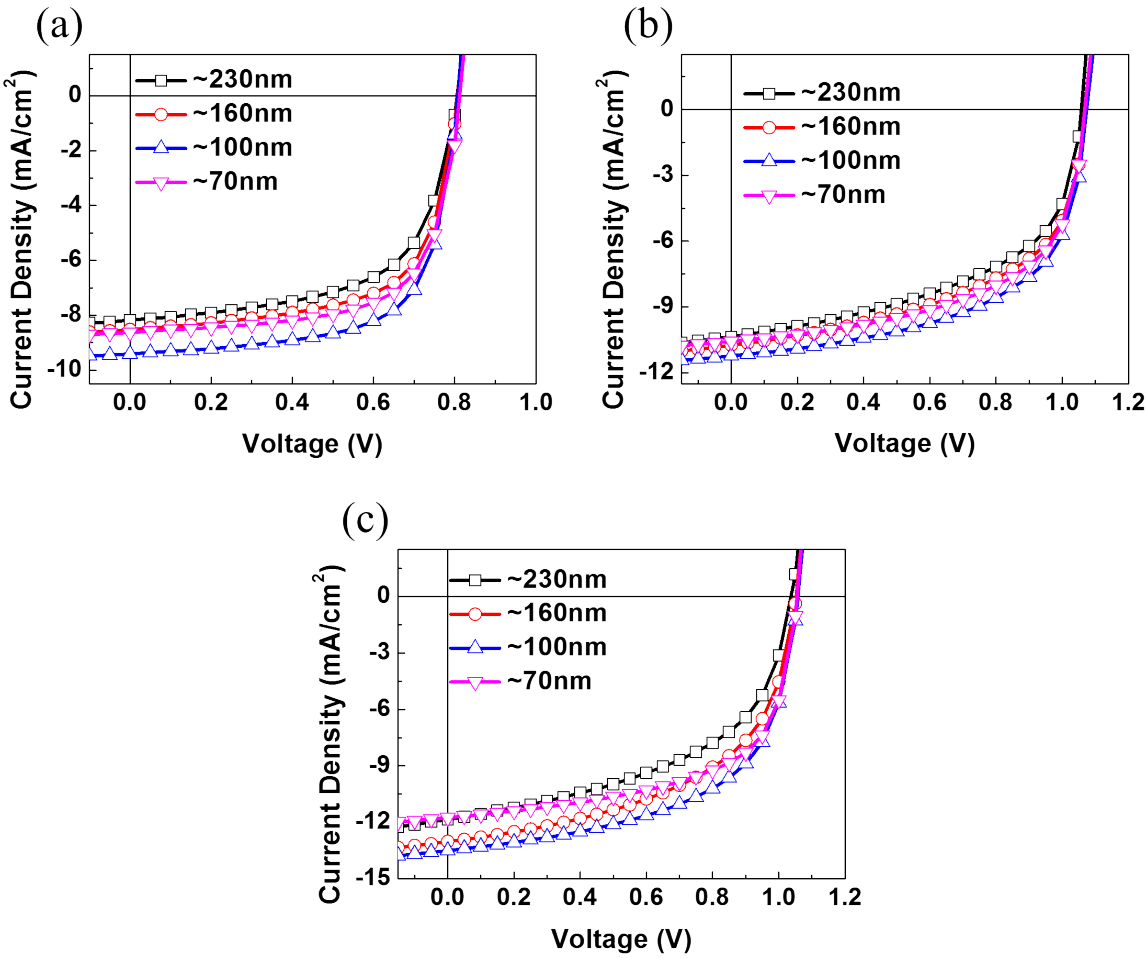

Figure S13. *J-V* curves with differnet thickness of the photoactive layer employing (a) P1:BTDT2R, (b) P2:BTDT2R and (c) P3:BTDT2R.

Table S11. Photovoltaic parameters of P3TH(P1):PTB7-Th(P3):BTDT2R-based ternary-blend OSCs.[a)]

Polymer Donor	Annealing	V_{OC} [V]	J_{SC} [mA/cm^2]	*FF* [%]	PCE [%]
P3HT(P1):PTB7-Th(P3) =0.0:2.0	As-cast	1.06	12.06 (11.90)[b)]	40	5.03 (4.90)[c)]
	SVA	1.06	13.52 (13.14)[b)]	57	8.19 (8.06)[c)]
P3HT(P1):PTB7-Th(P3) =0.5:1.5	As-cast	0.89	7.74 (7.62)[b)]	35	2.43 (2.28)[c)]
	SVA	0.87	9.94 (9.79)[b)]	50	4.37 (4.24)[c)]
P3HT(P1):PTB7-Th(P3) =1.0:1.0	As-cast	0.86	6.70 (6.60)[b)]	45	2.59 (2.48)[c)]
	SVA	0.81	9.43 (9.28)[b)]	57	4.33 (4.18)[c)]
P3HT(P1):PTB7-Th(P3) =1.5:0.5	As-cast	0.87	5.65 (5.60)[b)]	45	2.19 (2.06)[c)]
	SVA	0.81	9.19 (9.04)[b)]	61	4.49 (4.31)[c)]
P3HT(P1):PTB7-Th(P3) =2.0:0.0	As-cast	0.88	6.44 (6.27)[b)]	48	2.74 (2.66)[c)]
	SVA	0.81	9.42 (9.28)[b)]	67	5.09 (4.97)[c)]

[a)]The devices architecture is ITO/ZnO NPs/PEIE/photoactive layer(d = ~100nm)/MoO_X/Ag.

[b)]The value is calculated from EQE data.

[c)]The average PCE in the brackets is obtained from over 10 independent devices.

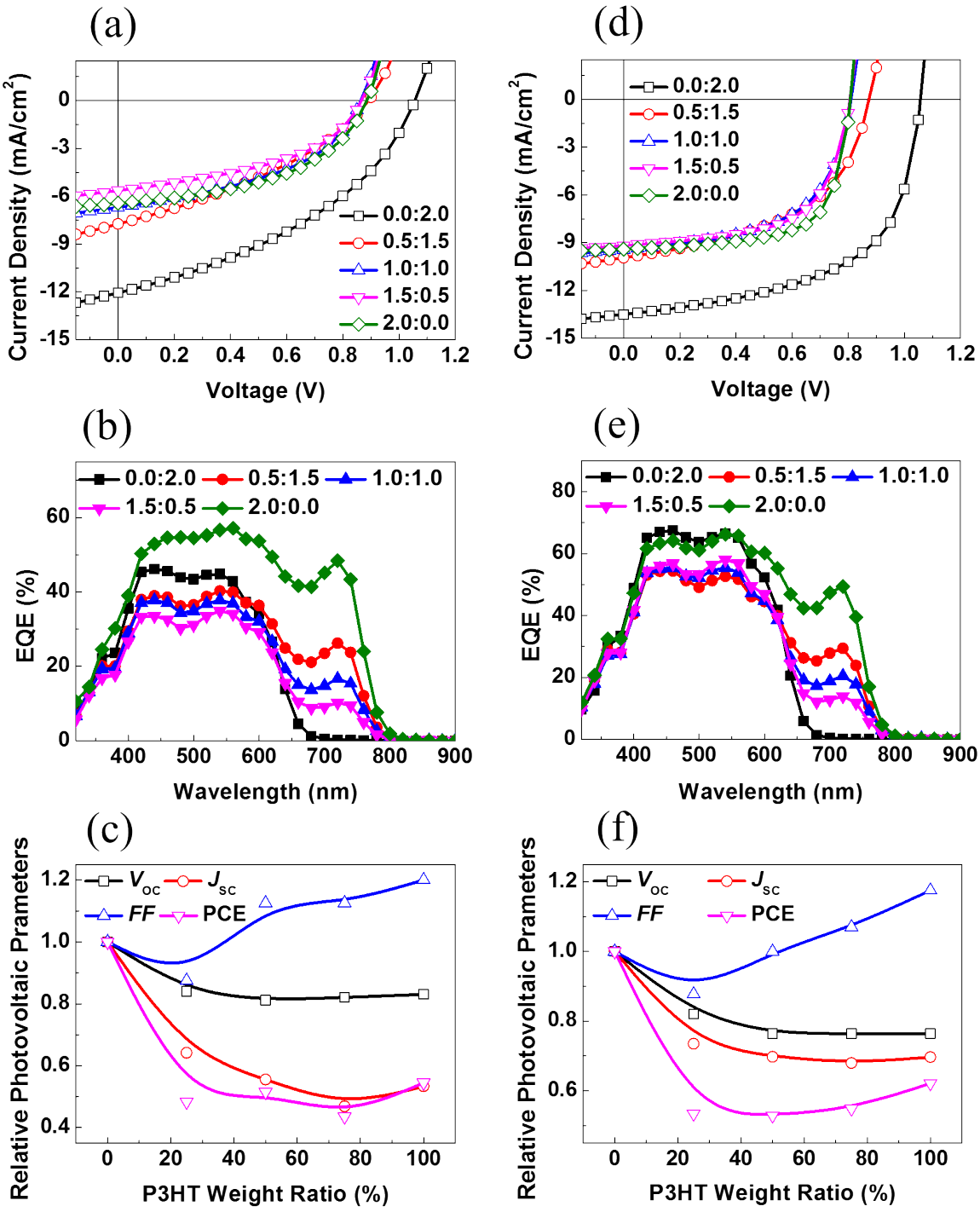

Figure S14. P3HT(P1):PTB7-Th(P3):BTDT2R-based ternary-blend OSCs of (a,d) *J-V* curves without and with SVA, (b,d) EQE graph without and with SVA, (c,f) Dependenc of P3HT weight ratio of V_{OC}, J_{SC}, *FF* and PCE parameters.

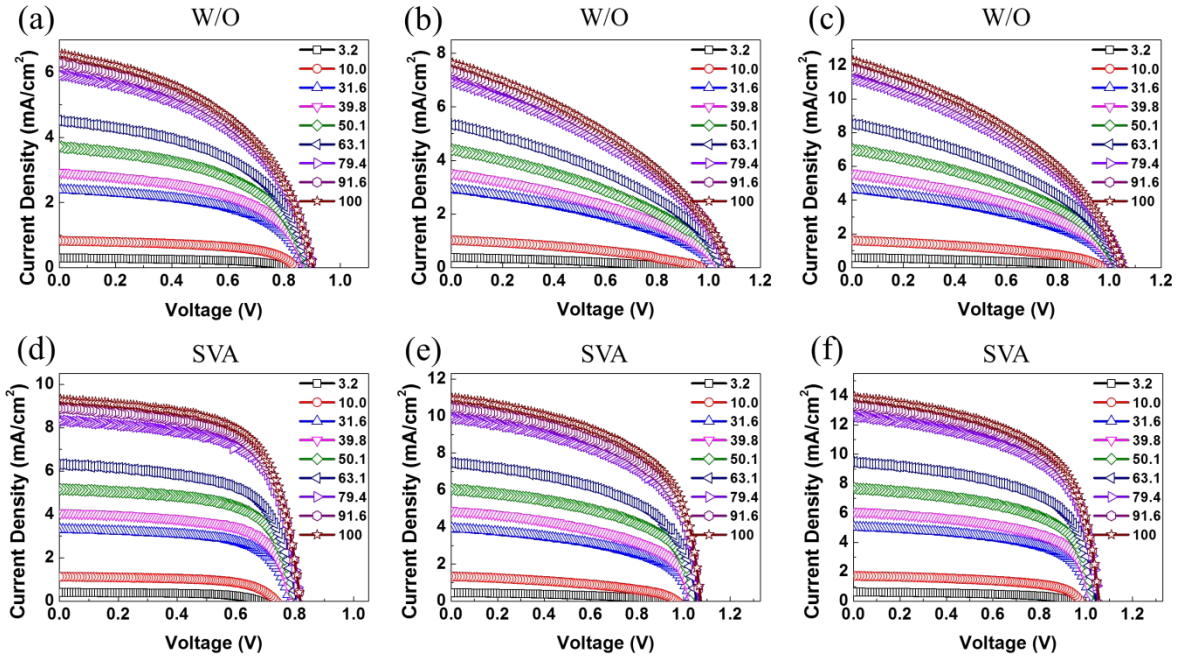

Figure S15. Light intensity-dependent *J-V* curves for the (a) neat (d) solvent vpor annealing of P1:BTDT2R, (b) neat (e) solvent vapor annealing of P2:BTDT2R and (c) neat (f) solvent vapor annealing of P3:BTDT2R-based OSCs.

Table S12. Hole and electron mobility of the polymer donors and BTDT2R acceptor without and with SVA.

Film	Annealing	μ_h [$cm^2/V\ s$][a)]	μ_e [$cm^2/V\ s$][b)]
P3HT	W/O	1.96×10^{-4}	-
	SVA[c)]	2.25×10^{-4}	-
PPDT2FBT	W/O	2.42×10^{-4}	-
	SVA[c)]	2.87×10^{-4}	-
PTB7-Th	W/O	5.05×10^{-4}	-
	SVA[c)]	5.25×10^{-4}	-
BTDT2R	W/O	-	7.30×10^{-6}
	SVA[c)]	-	5.14×10^{-5}

[a)]Hole-only device is ITO/PEDOT:PSS/Film/Au.

[b)]Electron-only device is ITO/ZnO NPs/PEIE/Film/Ca/Al.

[c)]The film is annealed by solvent vapor annealing (SVA) using DCM, for 15s.

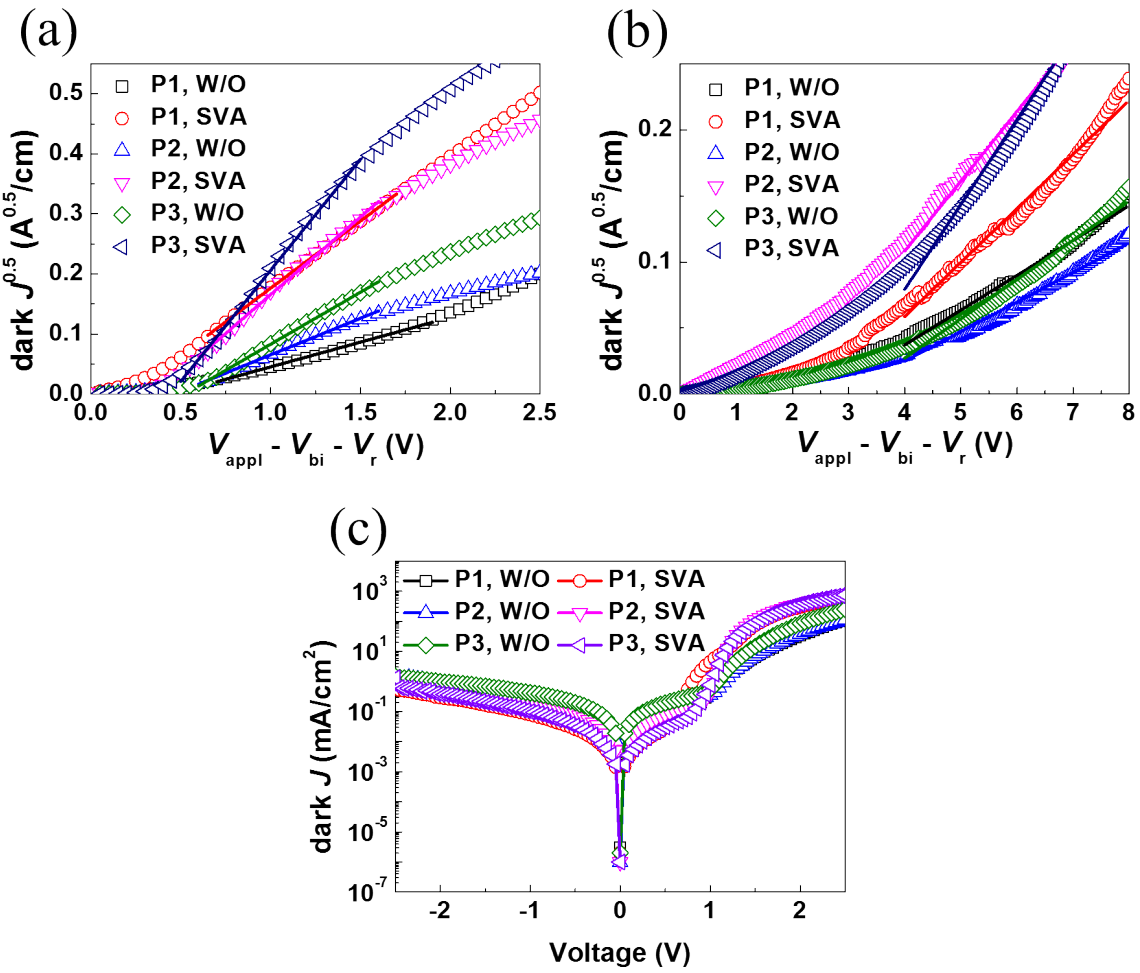

Figure S16. Dark $J^{0.5}$–V characteristics of (a) the hole-only devices with the structure of ITO/PEDOT:PSS/photoactive film/Au, (b) electron-only devices with the structure of ITO/ZnO NPs/PEIE/ photoactive film/Ca/Al. (c) Dark J-V curves of the OSCs without and with SVA.

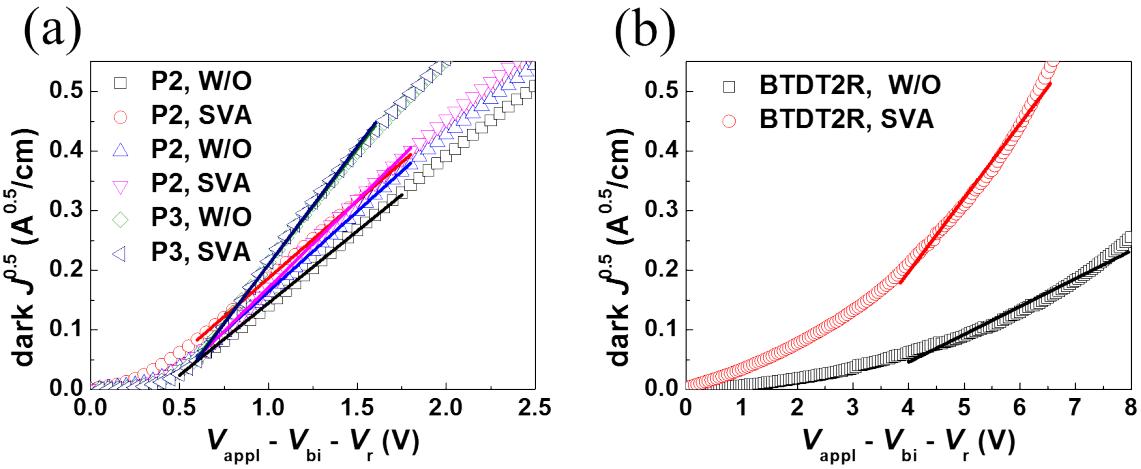

Figure S17. Dark $J^{0.5}$–V characteristics of (a) the hole-only devices with the structure of ITO/PEDOT:PSS/polymer/Au, (b) the electron-only devices with the structure of ITO/ZnO NPs/PEIE/BTDT2R/Ca/Al.

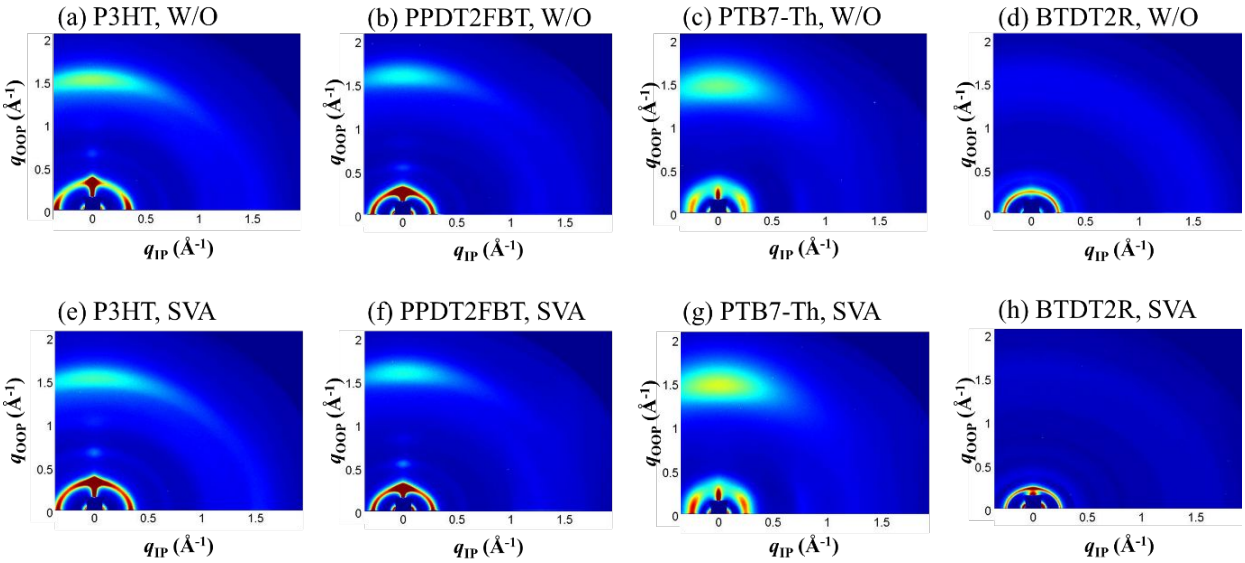

Figure S15. GIWAXS 2D scattering patterns of (a,e) P3HT without and with SVA, (b,f) PPDT2FBT without and with SVA, (c,g) PTB7-Th without and with SVA, (d,h) BTDT2R without and with SVA.

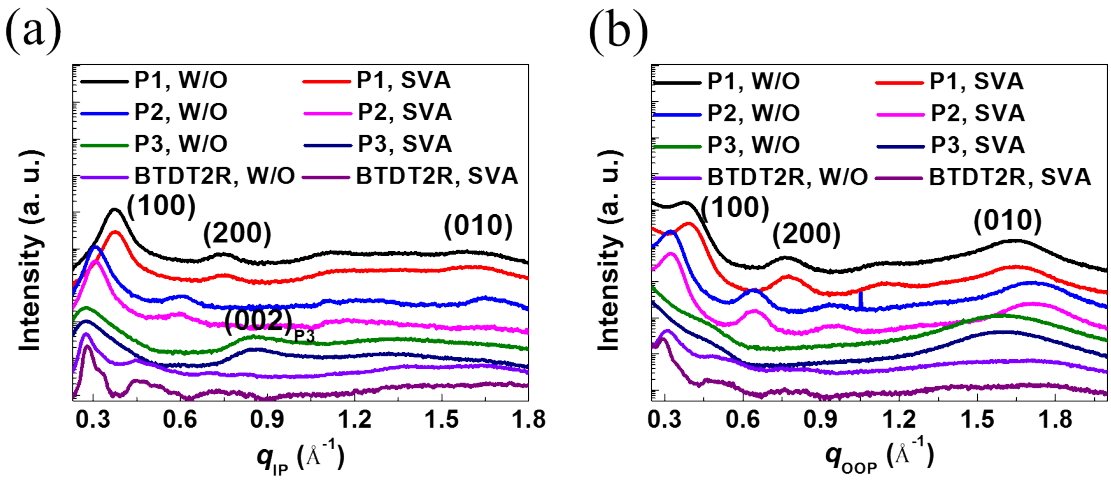

Figure S19. GIWAXS line profiles of polymer donors and BTDT2R without and with SVA of (a) in-pane and (b) out-of-plane directions.

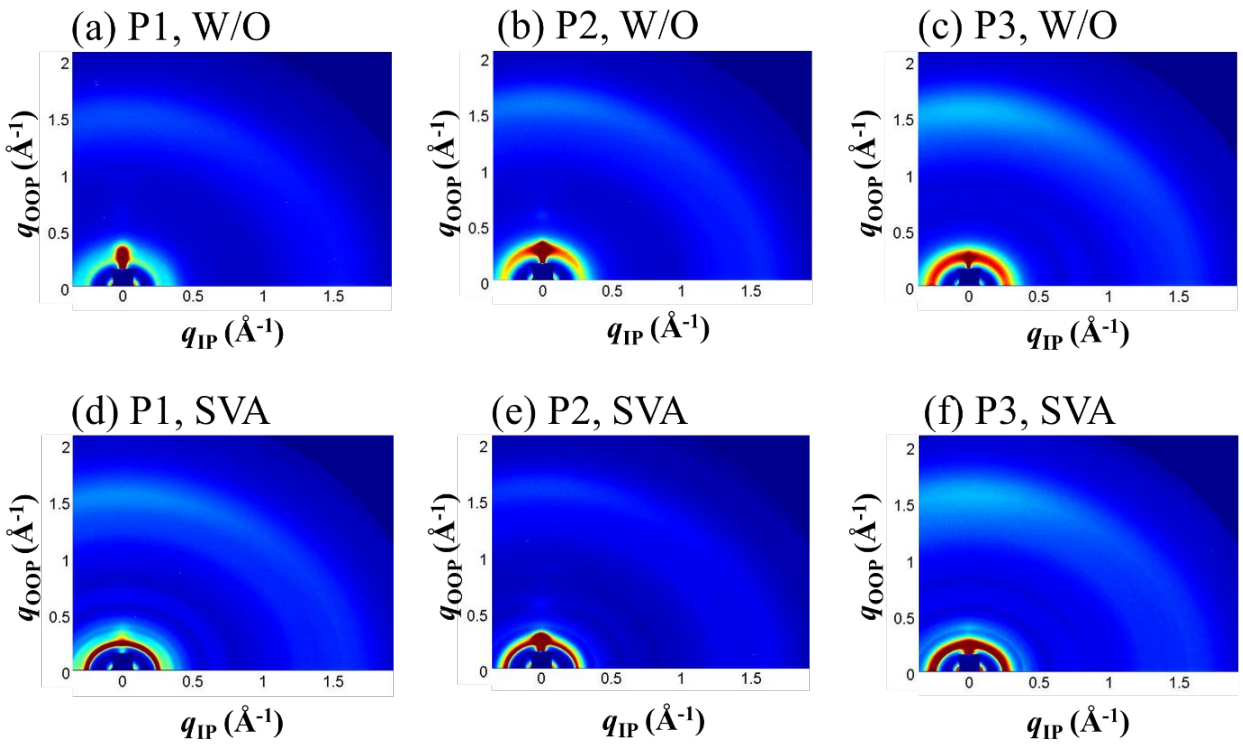

Figure S20. GIWAXS 2D scattering patterns of (a,d) P1:BTDT2R without and with SVA, (b,e) P2:BTDT2R without and with SVA, (c,f) P3:BTDT2R without and with SVA.

Table S13. Packing parameters of the active materials without and with SVA derived from GIWAXS measurements.

Film	Annealing	(100)[a] [Å]	(010)[a] [Å]	(100)[b] [Å]	(010)[b] [Å]
P3HT	W/O	15.72	3.81	16.87	-
	SVA[c]	15.98	3.78	16.87	-
PPDT2FBT	W/O	19.56	3.65	20.65	3.79
	SVA[c]	19.32	3.63	20.65	-
PTB7-Th	W/O	-	3.99	23.00	-
	SVA[c]	-	3.92	23.00	-
BTDT2R	W/O	20.30	-	22.72	-
	SVA[c]	21.26	-	22.72	-

[a]Calculation from OOP direction.

[b]Calculation from IP direction.

[c]The film is annealed by DCM, for 15s.

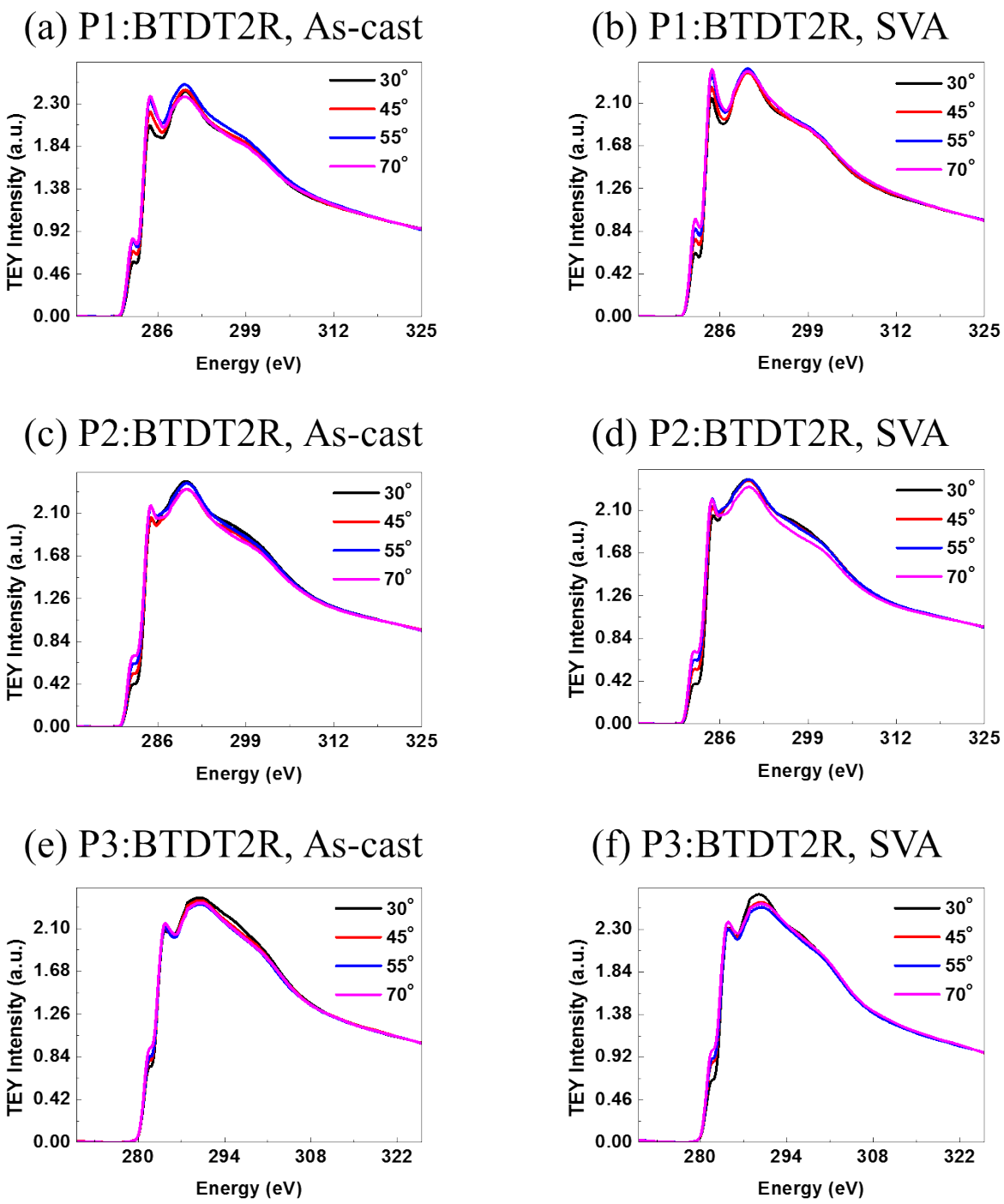

Figure S21. NEXAFS TEY mode of (a,b) P1, (c,d) P2 and (e,f) P3:BTDT2R blend films processed (a,c,e) without and (b,d,f) with SVA by different incidence angle.

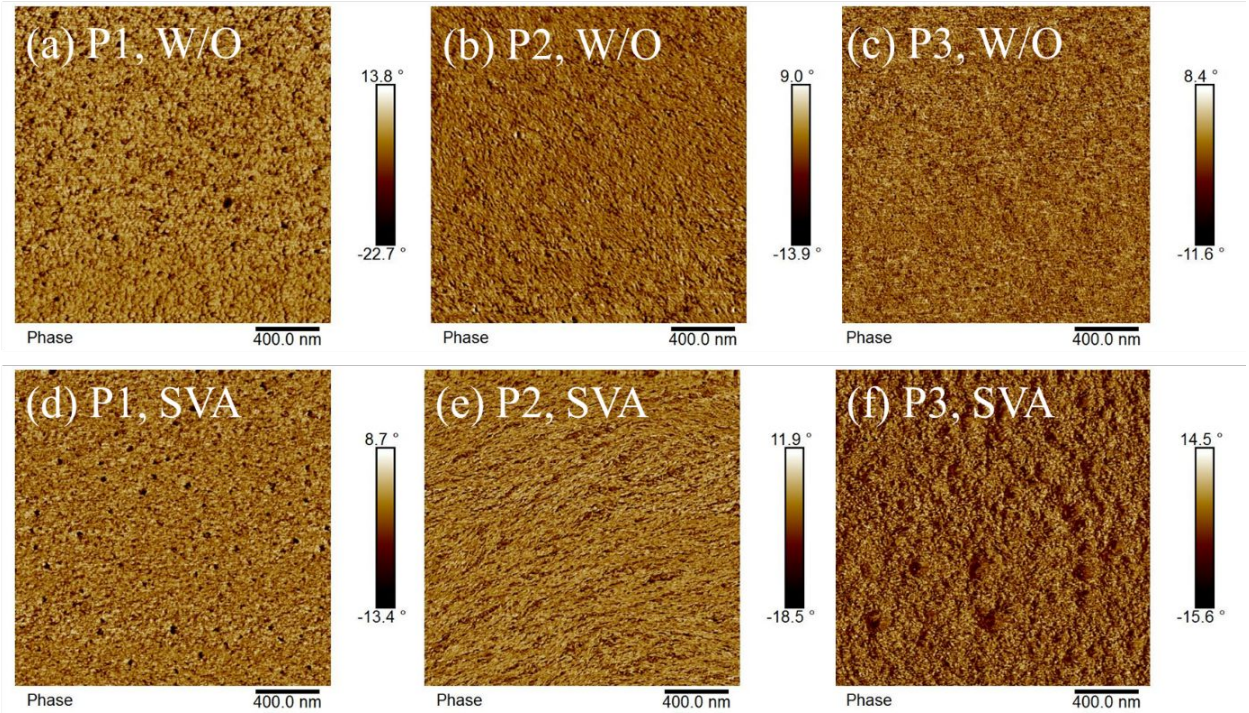

Figure S22. AFM phase images (a,d) P1:BTDT2R without and with SVA, (b,e) P2:BTDT2R without and with SVA, (c,f) P3:BTDT2R without and with SVA.